e-ISSN: 2289-649X

Available online at
https://journal.uitm.edu.my/ojs/index.php/SRJ

Scientific Research Journal 23(1) 2026, 35 – 53

Scientific Research Journal

First-Principles Study to Investigate the Structural, Electronic, Magnetic, and Mechanical Properties of Sn-Based Hydride Perovskites $XSnH_3$(X = Li, Na, K) for Hydrogen Storage Application

Nur Aqilah Zamri[1], Ahmad Fairoz Aziz[2], Nur Hafiz Hussin[3*], Mohd Hazrie Samat[4], Mohamad Fariz Mohamad Taib[5], Oskar Hasdinor Hassan[6]

[1,2,3]*Faculty of Applied Sciences, Universiti Teknologi MARA, Cawangan Pahang, Kampus Jengka 26400 Jengka, Pahang, Malaysia*
[4]*Physics Section, School of Distance Education, Universiti Sains Malaysia, 11800 USM, Pulau Pinang, Malaysia*
[5]*Faculty of Applied Science, Universiti Teknologi Mara, 40450 Shah Alam, Selangor, Malaysia*
[6]*Ionic Materials and Devices (iMADE), Institute of Science, Universiti Teknologi MARA, 40450 Shah Alam, Selangor, Malaysia*
[5,6]*Faculty of Arts and Design, Universiti Teknologi Mara, 40450 Shah Alam, Selangor, Malaysia*

ARTICLE INFO

Article history:
Received 01 October 2025
Revised 09 December 2025
Accepted 12 January 2026
Online first
Published 01 March 2026

ABSTRACT

This work presents a first-principles density functional theory (DFT) investigation of the structural, electronic, magnetic, and mechanical properties of cubic hydride perovskites $XSnH_3$ (X = Li, Na, K) for hydrogen storage applications. All compounds crystallize in the Pm3m (#221) structure with negative cohesive energies, confirming thermodynamic stability. The optimized lattice constants increase systematically from LiSnH3 (4.20 Å) to $NaSnH_3$ (4.26 Å) and $KSnH_3$ (4.35 Å). Electronic band structures and density of states reveal metallic behavior with 0.00 eV band gaps, while spin-polarized calculations indicate antiferromagnetic ordering. Mechanical analysis shows that

[3*]Corresponding author. *E-mail address*: hafizhussin@uitm.edu.my

https://doi.org/10.24191/srj.v23i1.41624

Keywords:
First Principles
Density Functional Theory
Hydrogen Storage

DOI:
10.24191/srj.v23i1.41628

$KSnH_3$ is the hardest compound, $NaSnH_3$ exhibits the greatest toughness, and $LiSnH_3$ is relatively brittle. Gravimetric hydrogen storage capacities were calculated as 2.35% (LiSnH3), 2.09% ($NaSnH_3$), and 1.88% ($KSnH_3$). Among them, LiSnH3 demonstrates the highest potential as a solid-state hydrogen storage medium. These findings provide new insights into the structure–property relationships of Sn-based hydride perovskites and establish their promise as candidates for next-generation hydrogen storage technologies.

1. INTRODUCTION

The global population growth and rapid urbanization have caused unsustainable energy usage and fossil fuel depletion [1]. The combustion of fossil fuels emits substantial quantities of carbon dioxide (CO_2), the primary greenhouse gas responsible for contributing to climate change and global warming [2]. The greenhouse effect is intensifying, and climate warming is accelerating due to increased fossil fuel consumption, leading to unprecedented CO_2 emissions [1, 3]. Consequently, CO_2 emissions from fossil fuels have become a significant environmental concern, linked to global warming and ecological degradation. In 1990, CO_2 emissions were 20.7 x 10^9 tons; by 2009, they had surprisingly reached 32.5 x 10^9 tons. Ecosystem depletion is a concern due to fossil fuel use [4]. Decarbonizing the energy supply through alternative, clean, sustainable, and renewable energy sources is essential to ensure energy sustainability and global security. Renewable energy (RE) resources are predicted to greatly impact the clean energy transition [5]. Hydrogen and other renewable energy sources are gaining popularity due to their efficiency and carbon-free production. Storing stable hydrogen or hydrogen molecules as a gas or compound in a hydrogen storage medium is a major difficulty in commercial hydrogen energy use [6]. The perovskite-type hydride is considered a potential candidate for solid-state hydrogen storage materials in the future [7]. ABX_3 represents perovskite compounds, where A and B are cations, and X is an anion. Halogen, oxygen, nitrogen, and fluorine can replace element X in ABX_3. Hydrogen storage materials usually have these traits: (i) These materials have strong hydrogen bonding, (ii) These materials store a lot of hydrogen due to their bulk, (iii) Catalytic properties improve hydrogen absorption in certain materials. These materials exhibit good gravimetric hydrogen storage, thereby enhancing their hydrogen storage capacity [4]. Discovering and analyzing renewable energy sources that meet society's needs while protecting the environment is vital. Ocean, wind, and geothermal energy are also options. These sources are inefficient and hard to manage, making them difficult to use. The ability of such sources to protect the environment, ensure safety, and adapt is being challenged, making their use difficult [4].

Researchers' focus has recently shifted to hydride perovskites of transition metals. Usman et al. [8] investigated the physical properties of $XGaH_3$ (X = K, Li), which exhibited metallic characteristics and could store hydrogen with 0.89 wt.% ($KGaH_3$) and 1.86 wt.% ($LiGaH_3$) hydrogen content. Rafique et al. [9] studied all compounds of $XCoH_3$ (X = In, Mn, Sr, Sn, Cd), which possess great physical properties and hydrogen storage capacities with 1.71%, 2.59%, 2.03%, 1.68%, and 1.74 wt.%, respectively. The study of formation energy, elastic properties, and phonon dispersion curves by Xu et al. [10] revealed that $XTiH_3$ (X = K, Rb, Cs) were mechanically, thermodynamically, and dynamically stable with hydrogen storage capabilities of 3.36%, 2.22%, and 1.65 wt.% at 209, 161, and 107 K hydrogen desorption temperatures,

respectively. Ali et al. [11] found that lithium-based hydride perovskites ($LiSH_3$ and $LiSeH_3$) exhibit metallic electronic behavior, thermodynamic stability at 300 K, promising optical responses, and significant hydrogen storage capacities, with $LiSH_3$ showing higher gravimetric and volumetric performance, suggesting their potential as sustainable hydrogen storage materials. A study by Talukder & Islam [12] indicated that $ARhH_3$ (A = Mg, Ca, Sr) perovskite hydrides were stable metallic conductors with good optical responses, ductile behavior, and practical hydrogen storage performance. They have gravimetric capacities of 1.56 – 2.34 wt.% and volumetric capacities of 93.36 – 117.65 g H_2/L. According to Hammad et al. [13]'s analysis, $XZrH_3$ (X = Na, Cs) perovskite hydrides are stable, metallic materials with anisotropic and nonmagnetic properties. They have significant hydrogen storage capacities (2.51% and 1.31 wt.%), indicating their potential as efficient candidates for hydrogen storage. DFT studies on $XInH_3$ (X = Rb, Cs) by Ahmed et al. [14] revealed stable, metallic, anisotropic cubic hydrides with low hydrogen storage capacities (1.45 – 1.18 wt.%), UV optical absorption, and mechanical brittleness, suggesting potential integration into solid-state hydrogen storage systems. $XNiH_3$ (X = Li, Na, K) perovskites investigated by Koufi et al. [15] exhibited stable cubic structures, metallic behavior, and promising hydrogen storage capacities (2.98 – 4.37 wt.%), suggesting their potential as multifunctional materials for hydrogen storage. $BeXH_3$ (X = Si, Ge) hydride perovskites, studied by Afaq et al. [16], exhibited mechanical, dynamic, and thermal stability, with favorable thermodynamic behavior and high hydrogen storage capacities (7.02 wt.% for $BeSiH_3$), indicating potential for hydrogen storage applications, as confirmed by DFT studies. Tahir et al. [4] served as the primary reference for this study, as we investigated the same metal hydride compound, $XSnH_3$ (X = Li, K), but with a more in-depth examination of Na in this study. We employed three different functionals: Local Density Approximation (LDA) method combined with the Ceperley–Alder–Perdew–Zunger (CA-PZ), Generalized Gradient Approximation, Perdew–Burke–Ernzerhof (GGA PBE), and Generalized Gradient Approximation Perdew–Burke–Ernzerhof for solids (GGA PBEsol).

This study employs first-principles density functional theory (DFT) calculations to investigate the structural, electronic, magnetic, and mechanical properties of $XSnH_3$ (X = Li, Na, K) hydride perovskites. The objectives are twofold: (i) to evaluate the stability and fundamental physicochemical characteristics of these compounds, and (ii) to assess their hydrogen storage capacity through gravimetric analysis. A comprehensive understanding of these properties is essential to identify the most suitable candidate for hydrogen storage applications and to advance the development of sustainable hydrogen-based energy technologies.

2. METHODOLOGY

2.1 Computational Methods

First-principles calculations were employed to investigate the structural, electronic, magnetic, and mechanical properties of $XSnH_3$ (X = Li, Na, K) hydride perovskites. All simulations were carried out using the Material Studio 2020 version 20.1 software by BIOVIA and the Cambridge Serial Total Energy Package (CASTEP) code [4, 17, 18]. The exchange–correlation energy was treated within the generalized gradient approximation (GGA) using the Perdew–Burke–Ernzerhof (PBE) functional with ultra-soft pseudopotentials. The Kohn–Sham equations were solved within the plane-wave pseudopotential framework, while periodic boundary conditions were applied to the set of wave-plane basis according to Bloch's theorem [19, 20].

https://doi.org/10.24191/srj.v23i1.41628

Structural relaxations were performed using the Broyden–Fletcher–Goldfarb–Shanno (BFGS) minimization algorithm, which efficiently handles unconstrained nonlinear optimization problems. This approach provides accurate determination of the electronic wave functions and charge densities of crystalline materials. To accelerate convergence of the self-consistent field (SCF) cycles, Pulay density mixing was adopted. This iterative procedure linearly combines density matrices from previous iterations, improving SCF stability, particularly for metallic systems with slow electronic convergence [21, 22].

To improve calculation accuracy and speed, a convergence test is being done. The test was vital to the plane wave pseudopotential [23]. The cut-off energy for $XSnH_3$ (X = Li, Na, K) is 100 – 500 eV, and the k-point is stimulated from 1 x 1 x 1 to 8 x 8 x 8. The Brillouin zone was sampled using a Monkhorst–Pack k-point mesh of 6 × 6 × 6, and the plane-wave basis was truncated at an energy cutoff of 330, 410, and 280 eV for $XSnH_3$ (X = Li, Na, K), respectively. Despite the relatively low cut-off value, all three compounds were tested converged. Convergence thresholds were set to 5×10^{-7} eV/atom for total energy, 0.03 eV/Å for maximum force, and 0.1 GPa for maximum stress, with atomic displacements constrained to within 0.001 Å. The maximum number of SCF iterations was set at 1000.

The CASTEP calculations for $XSnH_3$ (X = Li, Na, K) were very fast, taking a total of 54.70 s, 54.70 s, and 28.05 s, respectively. They were also very efficient, with parallel efficiencies of 96–98% using an 8-way k-point distribution, demonstrating great scalability and the optimal use of CPU power.

Structural and electronic properties were examined using the LDA-CAPZ, GGA-PBEsol, and GGA-PBE functionals to compare the results with those in Tahir et al. [4] and determine the best exchange-correlation functional of $XSnH_3$ (X = Li, Na, K) for further calculations in this study. Meanwhile, mechanical stability and elastic properties were primarily determined using the GGA-PBE functional, as previously established based on structural and electronic properties. The varied properties were tested to elucidate and determine the physical properties and hydrogen storage capabilities of $XSnH_3$ (X = Li, Na, K).

The cohesive energy (E_{co}) of each compound was calculated prior to further computations to evaluate its properties and material stability using Eq. (1) [24].

$$E_{co} = [E_{XSnH_3}^{Total} - mE_{Sn}^{bulk} - nE_{X}^{bulk} - oE_{H}^{bulk}] \quad (1)$$

where E_{Sn}^{bulk}, E_{X}^{bulk}, and E_{H}^{bulk} represent the free-state energies of Sn, X (Li, Na, K), and H atoms, respectively, while $m, n,$ and o denote the number of atoms in the system. The second-order elastic constants were calculated using the finite strain method, with each strain applied eight times to ensure accuracy. After full unit cell optimization, all relevant structural, electronic, magnetic, and mechanical properties were systematically evaluated [4].

https://doi.org/10.24191/srj.v23i1.41628

3. RESULTS AND DISCUSSION

3.1 Structural Properties

The structural characteristics of perovskite-type hydrides $XSnH_3$ (X = Li, Na, K) were analyzed following structural optimization. All compounds crystallize in the cubic Pm3m space group (#221). The optimized atomic positions are as follows: the X atom (Li, Na, K) occupies the corner of the unit cell at (0.0, 0.0, 0.0), Sn resides at the body center at (0.5, 0.5, 0.5), and H atoms are located at the face centers at (0.5, 0.5, 0.0). The corresponding crystal structure is shown in Fig. 1.

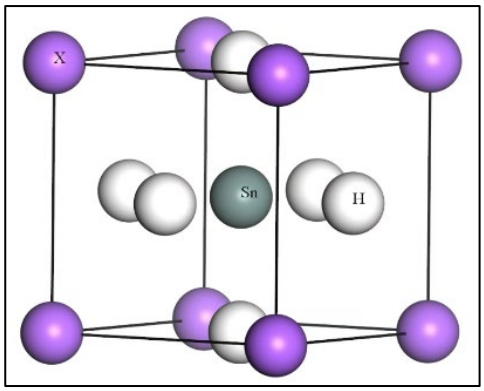

Fig. 1. The hydride perovskite's crystal structure of $XSnH_3$ (X = Li, Na, K)

The calculated lattice constants, unit cell volumes, and band gaps obtained using different exchange–correlation functionals (LDA-CAPZ, GGA-PBE, and GGA-PBEsol) are summarized in Table 1. Additionally, the calculated percentage errors in Table 1 were compared with current work data and previous published theoretical data to validate and demonstrate the reliability and validity of the results for future work.

Table 1. Comparison of lattice constant (Å), volume (Å^3), and band gap (eV) of $LiSnH_3$, $NaSnH_3$, and $KSnH_3$ with three different functionals: LDA-CAPZ, GGA-PBE, and GGA-PBEsol.

Functional		Compound	Lattice constant (Å) (a = b =c)	Volume (Å^3)	Band gap (eV)
Theoretical Data [4]$_a$					
GGA	PBE	$LiSnH_3$	4.10	68.92	0
		$KSnH_3$	4.30	79.50	0
CASTEP Calculation					
LDA	CAPZ	$LiSnH_3$	4.07(-0.73%)$_a$	67.27(-2.39%)$_a$	0
		$NaSnH_3$	4.11	69.38	0

https://doi.org/10.24191/srj.v23i1.41628

		$KSnH_3$	4.16(-3.26%)$_a$	71.98(-9.46%)$_a$	0
		$LiSnH_3$	4.19(2.20%)$_a$	73.36(6.44%)$_a$	0
GGA	PBEsol	$NaSnH_3$	4.24	75.96	0
		$KSnH_3$	4.30(0%)$_a$	79.70(0.25%)$_a$	0
		$LiSnH_3$	4.20(2.44%)$_a$	74.19(7.65%)$_a$	0
GGA	PBE	$NaSnH_3$	4.26	77.14	0
		$KSnH_3$	4.35(1.16%)$_a$	82.18(3.37%)$_a$	0

[a] Theoretical data [4]

Among these, the GGA-PBE functional yields slightly larger lattice constants and volumes compared to LDA-CAPZ and GGA-PBEsol. Specifically, the optimized lattice constants are 4.20 Å, 4.26 Å, and 4.35 Å for $LiSnH_3$, $NaSnH_3$, and $KSnH_3$, respectively. Correspondingly, the unit cell volumes obtained from GGA-PBE are 74.19 Å^3, 77.14 Å^3, and 82.18 Å^3. As expected, the volume increases with the larger ionic radii of the alkali atoms, with $KSnH_3$ exhibiting the largest lattice constant and volume.

The calculated cohesive energies are –14.51 eV/atom ($LiSnH_3$), –14.80 eV/atom ($NaSnH_3$), and –14.84 eV/atom ($KSnH_3$). The large negative values confirm strong interatomic bonding and thermodynamic stability of the cubic phases [4]. As the alkali cation changes from Li to K, the lattice constant increases in line with the atomic number. This trend is attributed to differences in ionic radii and electronegativity of the alkali metals, which strongly influence electron cloud distribution and the interaction between Sn, H, and X atoms within the lattice [25].

3.2 Electronic Properties

The electronic band structures and total density of states (TDOS) of $LiSnH_3$, $NaSnH_3$, and $KSnH_3$ were calculated using three different exchange–correlation functionals: LDA-CAPZ, GGA-PBE, and GGA-PBEsol, as illustrated in Fig. 2, Fig. 3, and Fig. 4. The calculations were performed along the high-symmetry directions of the first Brillouin zone, namely Γ–F–Q–Z–Γ [26]. In all cases, the Fermi level was positioned at 0 eV, which is represented by the horizontal reference line in the band structure diagrams.

https://doi.org/10.24191/srj.v23i1.41628

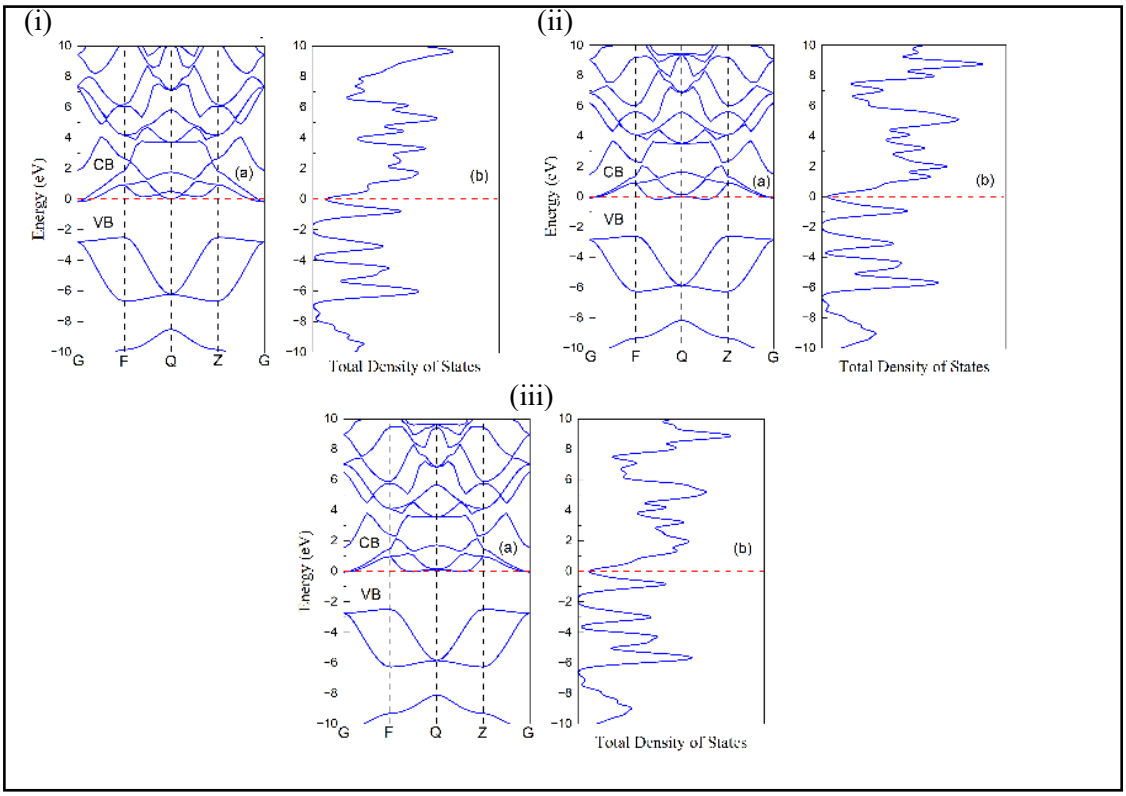

Fig. 2. (a) Band structure and (b) TDOS of $LiSnH_3$ with three distinct functionals: (i) LDA-CAPZ, (ii) GGA-PBE, and (iii) GGA-PBEsol

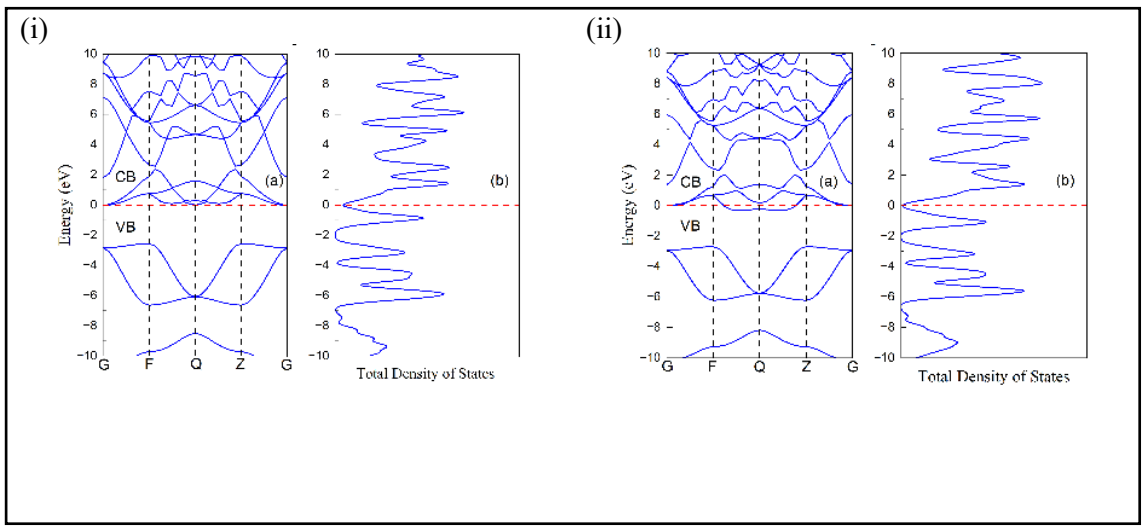

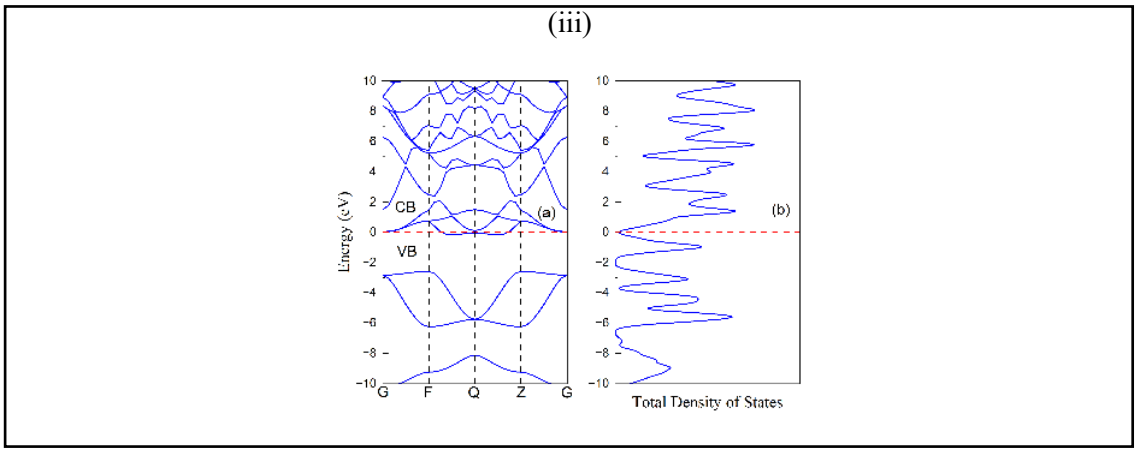

Fig. 3. Band structure and TDOS of $NaSnH_3$ with three distinct functionals: (a) LDA-CAPZ, (b) GGA-PBE, and (c) GGA-PBEsol.

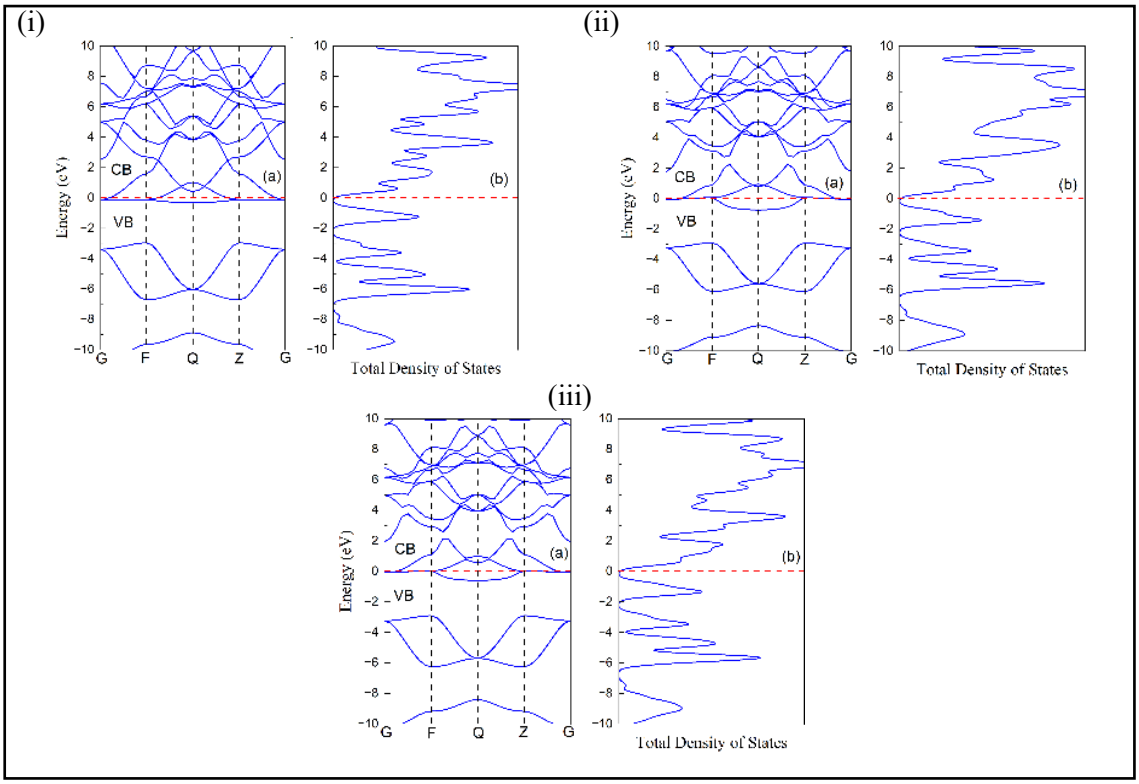

Fig. 4. Band structure and TDOS of $KSnH_3$ with three distinct functionals: (a) LDA-CAPZ, (b) GGA-PBE, and (c) GGA-PBEsol.

https://doi.org/10.24191/srj.v23i1.41628

For all three compounds, the valence band is located in the lower energy region, while the conduction band is situated at higher energies. The band gap corresponds to the energy difference between the maximum of the valence band and the minimum of the conduction band. However, for $LiSnH_3$, $NaSnH_3$, and $KSnH_3$, the valence and conduction bands overlap at the Fermi level, indicating the absence of a band gap. This overlap is consistent across all tested functionals, confirming the metallic character of the compounds [4]. Such metallicity is advantageous for hydrogen storage applications because it can enhance electronic conductivity, facilitating hydrogen absorption and desorption processes. Still, different energy band structures may occur when different cations (Li, Na, K) are present in the crystal lattice, as each cation has a distinct electronic configuration [27].

The TDOS values further support these observations. For $LiSnH_3$, the peak TDOS values for LDA-CAPZ, GGA-PBE, and GGA-PBEsol were 3.00, 3.49, and 3.28 electrons/eV at 9.65 eV, 8.77 eV, and 8.91 eV, respectively. In the case of $NaSnH_3$, the corresponding peak values were 2.79, 3.05, and 3.03 electrons/eV at 6.13 eV, 8.03 eV, and 8.08 eV. Meanwhile, for $KSnH_3$, the TDOS peaks were found to be 4.38, 4.74, and 4.56 electrons/eV at 7.31 eV, 6.90 eV, and 7.01 eV, respectively, for LDA-CAPZ, GGA-PBE, and GGA-PBEsol.

These results demonstrate that while overall metallic behavior is consistent, the magnitude and position of density of states (DOS) peaks vary slightly depending on the functional applied. This variation reflects the sensitivity of electronic states to the choice of exchange–correlation functional, but does not alter the general conclusion that $LiSnH_3$, $NaSnH_3$, and $KSnH_3$ exhibit metallic properties without a band gap.

A deeper understanding of the electronic structure of $XSnH_3$ (X = Li, Na, K) compounds can be obtained through the analysis of the partial density of states (PDOS), as presented in Fig. 5, Fig. 6, and Fig. 7. The PDOS provides information on the contributions of individual atomic orbitals to the overall electronic states and their role near the Fermi level. For $LiSnH_3$, calculations using all three functionals show that the valence band is dominated by contributions from the s-orbitals, while the conduction band is primarily derived from p-orbitals. A similar orbital distribution is observed in $NaSnH_3$, where the s-states govern the valence band, and the conduction band is largely influenced by p-states. In contrast, $KSnH_3$ exhibits a slightly different electronic configuration. The conduction band is strongly influenced by both p- and d-orbital states, whereas the valence band shows significant contributions from s-states, with the s-character being more pronounced in this compound compared to $LiSnH_3$ and $NaSnH_3$. Overall, the simultaneous contributions of s-, p-, and d-states at the Fermi level confirm the metallic nature of all three compounds. The presence of such intermetallic character is particularly favorable, as it enhances electron mobility and enables these perovskite hydrides to effectively accommodate and release hydrogen. This characteristic suggests their potential as efficient solid-state hydrogen storage materials [28].

https://doi.org/10.24191/srj.v23i1.41628

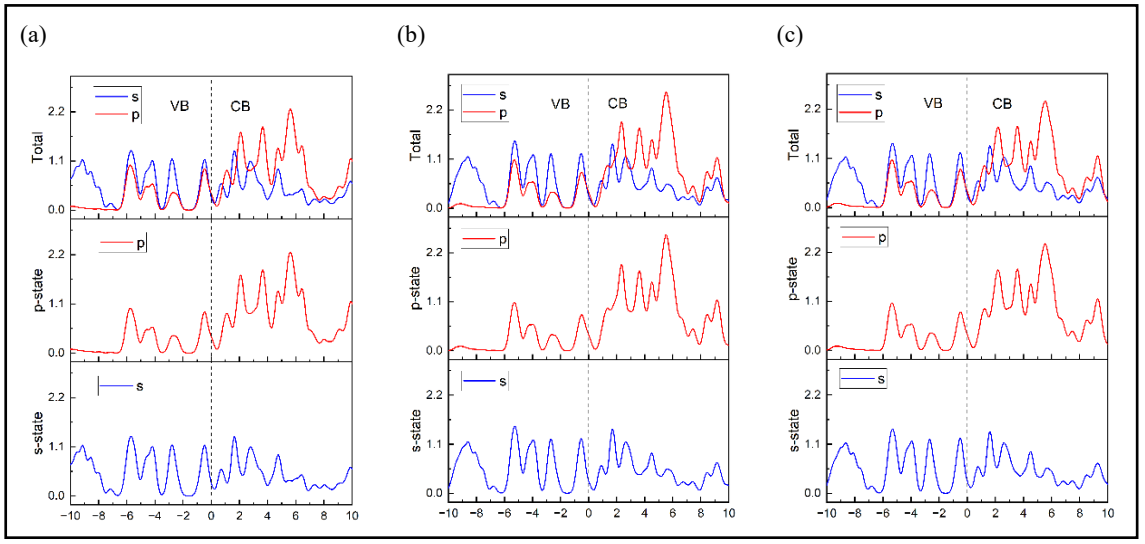

Fig. 5. PDOS of $LiSnH_3$ with three distinct functionals: (a) LDA-CAPZ, (b) GGA-PBE, and (c) GGA-PBEsol

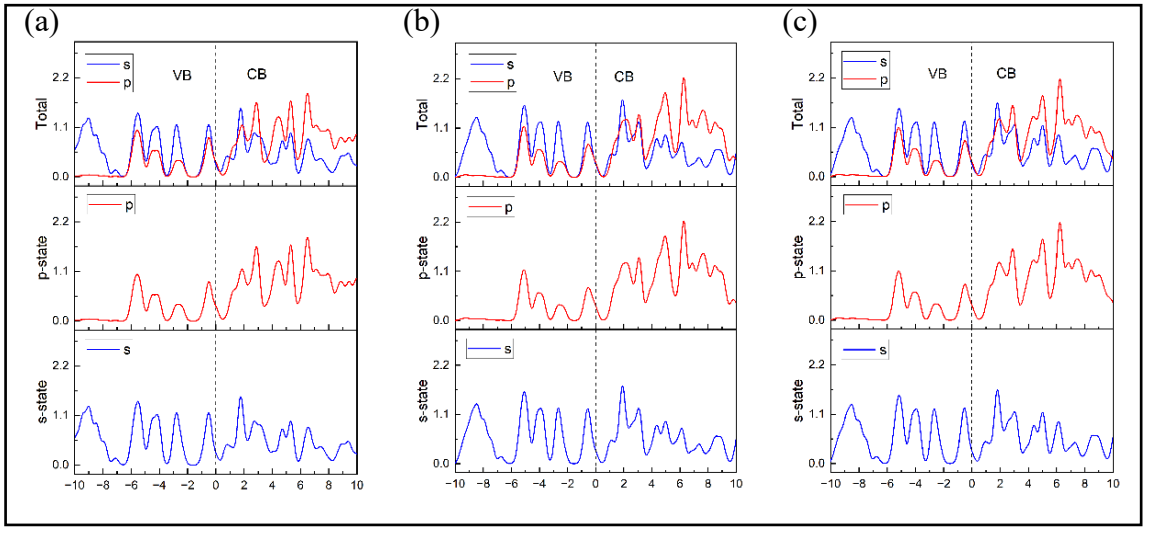

Fig. 6. PDOS of $NaSnH_3$ with three distinct functionals: (a) LDA-CAPZ, (b) GGA-PBE, and (c) GGA-PBEsol

https://doi.org/10.24191/srj.v23i1.41628

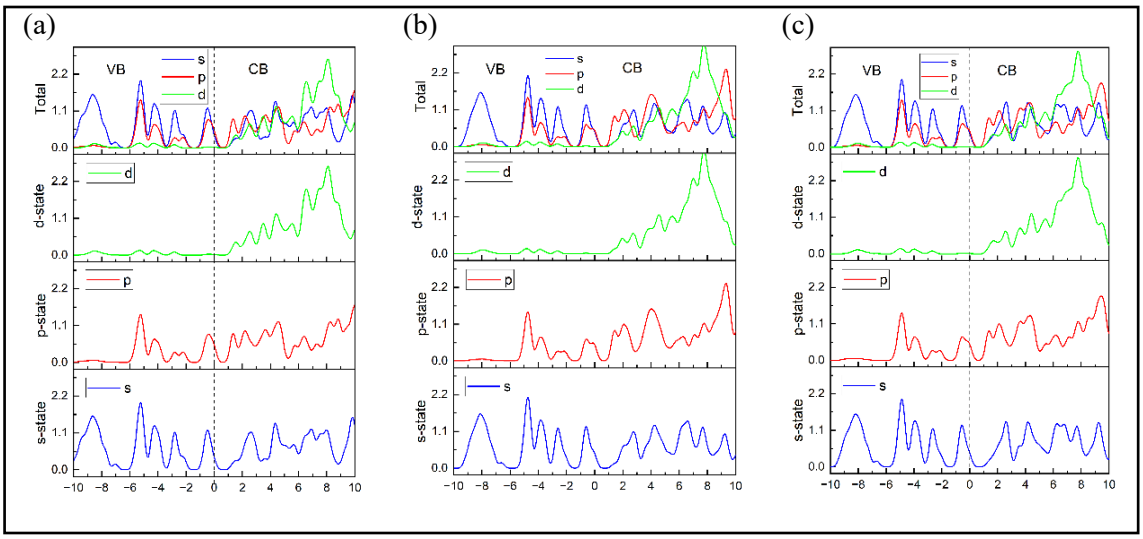

Fig. 7. PDOS of $KSnH_3$ with three distinct functionals: (a) LDA-CAPZ, (b) GGA-PBE, and (c) GGA-PBEsol

3.3 Magnetic Properties

The magnetic behavior of $XSnH_3$ (X = Li, Na, K) hydride perovskites was examined through spin-polarized band structure and density of states (DOS) calculations using the GGA-PBE functional. The spin-polarized band structures are shown in Fig. 8, while the corresponding spin-polarized DOS profiles are presented in Fig. 9. In these representations, red lines denote spin-up states and blue lines indicate spin-down states in the band structures, while in the DOS plots, black and red curves correspond to spin-up and spin-down contributions, respectively.

In all three compounds, the Fermi level is located at 0 eV, and the spin-up and spin-down states are symmetric about this level. This symmetry indicates that $LiSnH_3$, $NaSnH_3$, and $KSnH_3$ exhibit no net magnetization despite their metallic characteristics. The overlap of valence and conduction bands confirms the metallic nature of the materials, which could improve the conductivity of the compounds, while the symmetric spin distribution demonstrates antiferromagnetic ordering [28].

https://doi.org/10.24191/srj.v23i1.41628

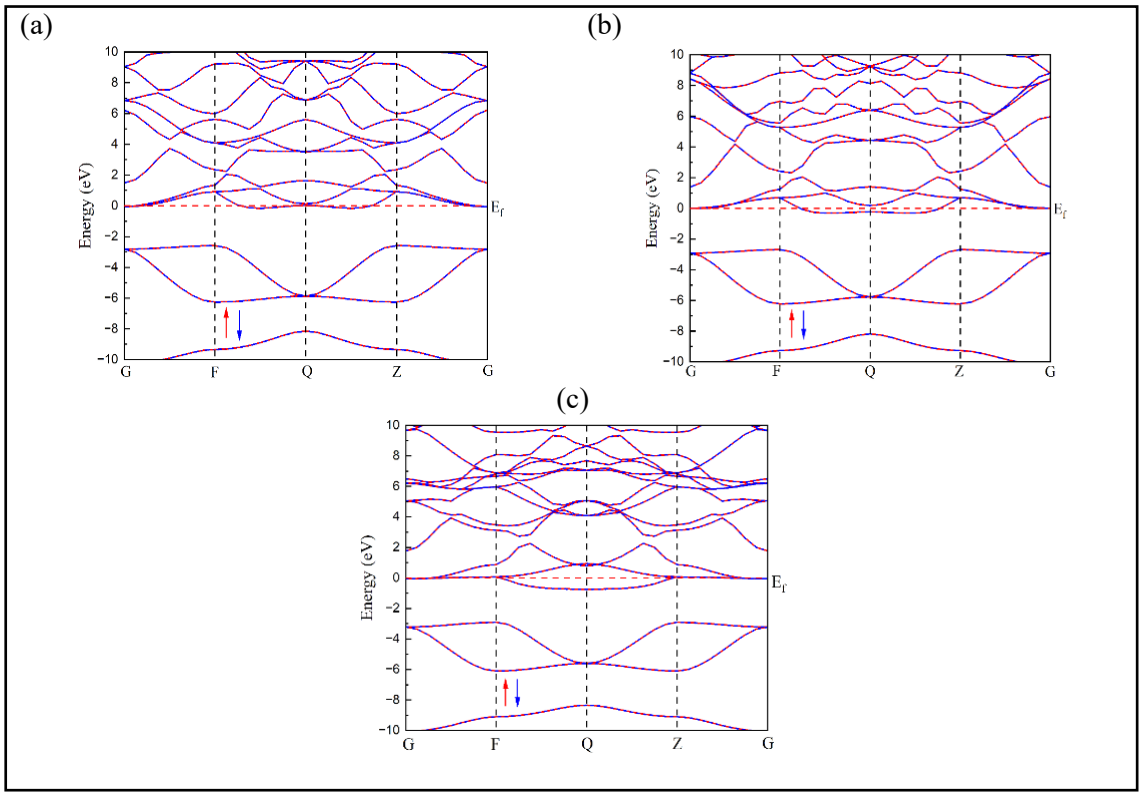

Fig. 8. Spin-polarized band structure of (a) $LiSnH_3$, (b) $NaSnH_3$, and (c) $KSnH_3$

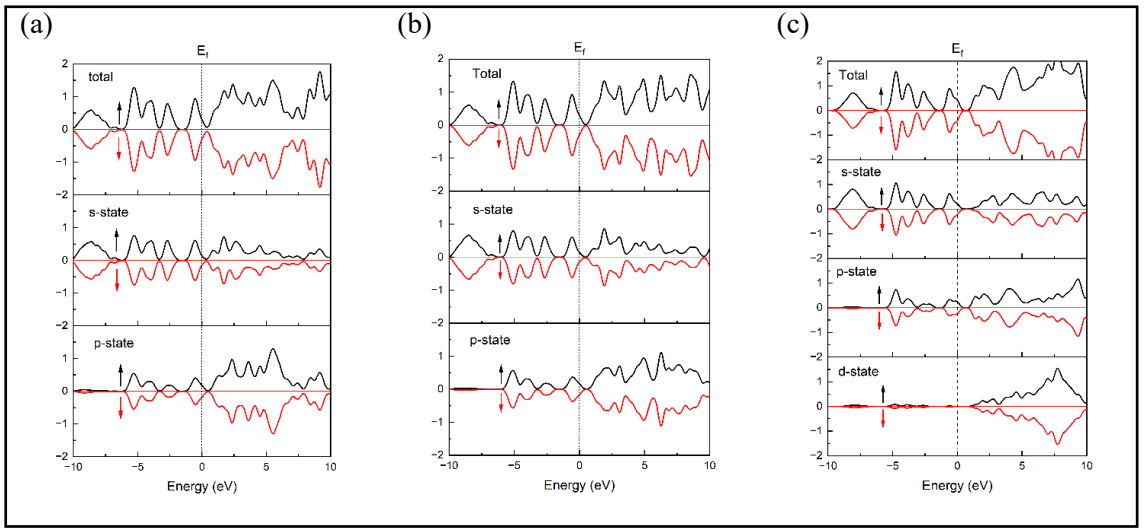

Fig. 9. Spin-polarized total and partial density of states of (a) $LiSnH_3$, (b) $NaSnH_3$, and (c) $KSnH_3$

https://doi.org/10.24191/srj.v23i1.41628

Further insight is obtained from the spin-polarized PDOS (Fig. 9), where mirror-image relationships between spin-up and spin-down states are evident across the s-, p-, and d-orbitals. This symmetric distribution reflects the complete cancellation of magnetic dipoles, confirming that all three compounds exhibit antiferromagnetic behavior [4]. The origin of this behavior can be attributed to the balanced electronic occupancy of the valence states, where the contributions of spin-up and spin-down electrons are equal, resulting in zero net magnetization. In particular, the hybridization between Sn–H orbitals and the alkali metal states produces delocalized electronic interactions that favor antiferromagnetic alignment. Due to the paired configuration of electron spins, a non-magnetic substance lacks any magnetic moments. Antiferromagnetic materials exhibit magnetic moments; however, the overall effect results in their cancellation, as neighbouring atoms position their spins in opposing directions (↑↓↑↓).

The antiferromagnetic metallic character is of particular interest because it combines high electronic conductivity with magnetic stability, a combination rarely observed in hydride perovskites. This dual characteristic enhances charge transport within the lattice while preventing spin polarization effects that could destabilize the system. Such behavior is advantageous for hydrogen storage applications, as metallic conductivity facilitates faster hydrogen absorption and desorption, while antiferromagnetic ordering ensures structural and magnetic stability under operating conditions [29]. Additionally, the presence of orbital hybridization near the Fermi level suggests that these compounds may exhibit tunable electronic properties in response to external perturbations, such as pressure, doping, or strain. This tunability could be exploited to further optimize their hydrogen storage performance and broaden their applicability in solid-state energy systems.

3.4 Mechanical Properties

The mechanical properties of $XSnH_3$ (X = Li, Na, K) hydride perovskites were evaluated using the elastic constants derived from first-principles calculations. The elastic response of a crystalline material can be described by its stiffness matrix, which in cubic systems reduces to three independent constants: C_{12}, C_{11}, and C_{44}, notation [30]. These constants govern the stability and resistance of the lattice against applied deformations. For cubic crystals, the Born–Huang stability criteria must be satisfied for mechanical stability and are expressed as in Eq. (2) [31].

$$C_{11} + 2C_{12} > 0;\ C_{11} - C_{12} > 0;\ C_{44} > 0 \tag{2}$$

The calculated elastic constants, as shown in Table 2, show that $KSnH_3$ fulfills the stability conditions with all positive values of C_{11}, C_{12}, and C_{44}. In contrast, $LiSnH_3$ and $NaSnH_3$ display slightly negative values of C_{44}, suggesting marginal mechanical instability under shear deformation. Nevertheless, the relatively large magnitudes of C_{11} and C_{12} indicate that these phases remain reasonably robust under compressive stresses [4].

Using the Voigt–Reuss–Hill (VRH) approximations, macroscopic mechanical moduli were derived, including the bulk modulus (B), shear modulus (G), and Young's modulus (E). These parameters provide further insight into the resistance of the compounds to compression, shear deformation, and tensile stress, respectively. The results reveal that $NaSnH_3$ possesses the highest bulk modulus, indicating superior

resistance to volumetric compression and hence greater toughness. $KSnH_3$, on the other hand, exhibits the largest shear and Young's moduli, making it the hardest among the three compounds. By contrast, $LiSnH_3$ demonstrates lower values of both shear and Young's moduli, consistent with its more brittle nature [25].

Ductility and brittleness were further assessed using Pugh's ratio (B/G) and Poisson's ratio (ν). Materials with B/G > 1.75 are generally classified as ductile, while those with lower ratios are considered brittle [29]. The calculated B/G values indicate that $NaSnH_3$ and $KSnH_3$ are ductile, whereas $LiSnH_3$ is brittle. Similarly, the Poisson's ratios for all compounds exceed 0.25, suggesting that ionic bonding dominates their lattice interactions.

The elastic anisotropy factor (A) was also evaluated to determine the directional dependence of elastic properties. A value of A = 1 corresponds to isotropic elasticity, whereas deviations from unity indicate anisotropy [31]. All three compounds exhibit anisotropic elastic behavior, which may influence their mechanical response under external stresses and could affect their performance in hydrogen storage systems subjected to cycling conditions.

Overall, these findings suggest that while $LiSnH_3$ is relatively brittle, $NaSnH_3$ provides the best balance of toughness and ductility, and $KSnH_3$ offers superior hardness. Such mechanical diversity highlights the tunability of $XSnH_3$ compounds and underscores the potential of tailoring their structural resilience for practical hydrogen storage applications.

Table 2. The elastic constant C_{ij} (GPa), anisotropic index A, bulk modulus, (GPa), shear modulus *G* (GPa), Young's modulus *E* (GPa), Poisson's ratio ν, and B/G ratio of $XSnH_3$ (X = Li, Na, K).

Parameters	**$LiSnH_3$**	**$NaSnH_3$**	**$KSnH_3$**
C12	3.84	6.31	4.41
C11	90.012	85.32	72.37
C44	-7.78	-0.77	6.18
A	-0.18	-0.020	0.18
B	32.56	32.65	27.06
GV	12.57	15.34	17.30
GR	-14.75	-1.30	9.18
G	-1.092	7.02	13.24
E	-3.31	19.65	34.15
ν	0.78	0.58	0.41
B/G	-29.82	4.65	2.044

https://doi.org/10.24191/srj.v23i1.41628

3.5 Hydrogen Storage Properties

Hydrogen storage remains one of the key challenges in the realization of a hydrogen-based energy economy. The efficiency of storage materials is commonly evaluated by their gravimetric hydrogen storage capacity (GHSC), which quantifies the mass fraction of hydrogen relative to the host compound [32]. Hydrogen can be stored either through physisorption, involving weak van der Waals interactions, or through chemisorption, which involves stronger chemical bonding. In metal hydrides, hydrogen typically forms ionic, covalent, metallic, or complex bonding interactions with the host lattice, influencing both the stability and reversibility of hydrogen uptake and release [33]. For perovskite-type hydrides such as $XSnH_3$ (X = Li, Na, K), the storage capacity is strongly influenced by the size and mass of the alkali cation, as well as the bonding environment with Sn and H atoms. The gravimetric hydrogen storage capacity was calculated using Eq. (3) [4].

$$C_{wt}\% = \left[\frac{pM_H}{M_{comp} + pM_H}\right] x100\% \quad (3)$$

where M_{comp} is the molar mass of the compound, M_H is the molar mass of hydrogen, and p is the number of hydrogen atoms per formula unit. Among the ABH_3-type perovskite compounds, those exhibiting hydrogen storage capabilities between 1.2 – 6.0 wt.% are highly interesting [34]. Based on this formulation, the calculated hydrogen storage capacities are 2.35%, 2.09%, and 1.88% for $LiSnH_3$, $NaSnH_3$, and $KSnH_3$, respectively. In comparison to Tahir et al. [4]'s studies, both studies demonstrated the same gravimetric hydrogen storage capacities, with the additional calculation of $NaSnH_3$. These results show a decreasing trend in hydrogen capacity with increasing atomic mass of the alkali metal. $LiSnH_3$ exhibits the highest gravimetric storage capacity due to the relatively low molar mass of Li compared with Na and K, which reduces the denominator in Eq. (3) and increases the hydrogen-to-compound mass ratio.

The presence of an intermetallic phase in these compounds, as indicated by the electronic structure analysis, enhances hydrogen absorption by providing favorable electronic states near the Fermi level [28]. Moreover, the metallic conductivity of these perovskites facilitates rapid charge transfer during hydrogen adsorption and desorption processes, further improving their potential as storage materials. Although the absolute hydrogen storage capacities of $XSnH_3$ are somewhat lower than those of some lightweight complex hydrides, their combination of thermodynamic stability, metallic conductivity, antiferromagnetic ordering, and reasonable gravimetric capacity positions them as promising candidates for solid-state hydrogen storage. In particular, $LiSnH_3$ stands out as the most effective among the series, offering the highest storage capacity and stable mechanical properties, which could be further enhanced through chemical doping, alloying, or nanostructuring strategies.

4. CONCLUSIONS

In this study, first-principles DFT calculations were employed to systematically investigate the structural, electronic, magnetic, mechanical, and hydrogen storage properties of cubic hydride perovskites $XSnH_3$ (X = Li, Na, K). All compounds were found to crystallize in the Pm3m (#221) cubic phase, characterized by negative cohesive energies, confirming their thermodynamic stability. Electronic structure calculations revealed that all compounds are metallic, with overlapping valence and conduction bands at the Fermi level.

https://doi.org/10.24191/srj.v23i1.41628

Spin-polarized DOS analysis demonstrated symmetric spin-up and spin-down states, indicating antiferromagnetic ordering. This antiferromagnetic metallic character is particularly attractive for hydrogen storage, as it combines high electrical conductivity with magnetic stability. It is easier for charges to move around in the lattice because it is metallic, which speeds up the uptake and release of hydrogen. On the other hand, the antiferromagnetic arrangement stops spin-polarization phenomena that could become unstable and helps keep the structure and magnetic integrity during operation. Mechanical analysis showed that $KSnH_3$ is the hardest material, $NaSnH_3$ possesses the greatest toughness, and $LiSnH_3$ is comparatively brittle. The Pugh's ratio and Poisson's ratio further suggested that $NaSnH_3$ and $KSnH_3$ are ductile, whereas $LiSnH_3$ tends toward brittleness. The mechanical diversity observed among these compounds highlights the strong influence of alkali substitution on their elastic response and resilience. Hydrogen storage assessments revealed gravimetric storage capacities of 2.35%, 2.09%, and 1.88% for $LiSnH_3$, $NaSnH_3$, and $KSnH_3$, respectively. Among the three, $LiSnH_3$ emerges as the most promising candidate due to its highest hydrogen capacity, favorable thermodynamic stability, and synergistic electronic properties. Overall, this work demonstrates that Sn-based hydride perovskites, particularly LiSnH3, hold significant potential as solid-state hydrogen storage materials. The combined insights into their structural, electronic, and mechanical behavior provide a foundation for the rational design and optimization of next-generation hydride-based storage systems. Future studies may explore doping, alloying, or strain engineering of other perovskite-type hydrides to further enhance their gravimetric hydrogen storage capacity, which could reach more than 5 wt.%. This could improve hydrogen storage performance and practical applicability. This work could also be used to evaluate the data experimentally in future work.

5. ACKNOWLEDGMENTS/FUNDING

Appreciation to Universiti Teknologi MARA (UiTM), Cawangan Pahang, Kampus Jengka and Ionic Materials & Devices (iMADE) Research Laboratory, Institute of Science, Universiti Teknologi MARA (UiTM) for the facilities provided.

6. CONFLICT OF INTEREST STATEMENT

The authors declare that this research was conducted in the absence of any commercial or financial relationships that could be construed as a potential conflict of interest.

7. AUTHORS' CONTRIBUTIONS

Nur Aqilah Zamri: Conceptualisation, methodology, formal analysis, investigation, data curation, visualisation, and writing–original draft: Nur Hafiz Hussin: Conceptualisation, methodology, formal analysis, investigation, data curation, visualisation, and writing–original draft.; Ahmad Fairoz Aziz: Methodology, writing–review and editing.; Mohd Hazrie Samat: Methodology, writing–review and editing.;Mohamad Fariz Mohamad Taib: Project administration, resources, software, validation.;Oskar Hasdinor Hassan: Project administration, resources, software, validation

8. DECLARATION OF GENERATIVE AI IN THE WRITING PROCESS

During the preparation of this work, the authors used ChatGPT to improve the clarity and language quality of the manuscript. After using this tool, the authors carefully reviewed and edited the content and take full responsibility for the content of the publication.

9. DATA AVAILABILITY/SUPPLEMENTARY MATERIALS

All data supporting the findings of this study are included within the article and its Supplementary Materials. The supplementary files provide detailed computational parameters, optimized lattice constants, elastic constants, formation energies, electronic structure results, and hydrogen storage-related properties derived from density functional theory (DFT) calculations. Raw computational input and output files are available from the corresponding author upon reasonable request to ensure full reproducibility of the results.

10. ETHICS STATEMENT

The authors declare that this research did not involve human or animal subjects. All computational procedures were performed following the institutional Safety, Health, and Environmental (HSE) guidelines of [UiTM].

11. REFERENCES

[1] H. Zhong, Z. Wang, Y. Zhang, S. Suo, Y. Hong, L. Wang & Y. Gan, 2024. Gas storage in geological formations: A comparative review on carbon dioxide and hydrogen storage, *Materials Today Sustainability*, 26, 100720.

[2] S. Wang, J. Liu, Z. Li, X. Wei, J. Luo, J. Tang, Y. Zhang, P. Wang, D. Wang, X. Wang, X. Hu & F. Zhang, 2024. Preparation and properties of hydrogen storage materials of porous carbon composite diatom skeleton, *International Journal of Hydrogen Energy*, 64, 773 – 780.

[3] S. Fawzy, A. I. Osman, J. Doran & D. W. Rooney, 2020. Strategies for mitigation of climate change: a review, *Environmental Chemistry Letters*, 18(6), 2069 – 2094.

[4] M. Tahir, M. Usman, J. U. Rehman & M. B. Tahir, 2024. A first-principles study to investigate the physical properties of Sn-based hydride perovskites $XSnH_3$ (X = K, Li) for hydrogen storage application, *International Journal of Hydrogen Energy*, 50, 845 – 853.

[5] F. Dawood, M. Anda & G. M. Shafiullah, 2020. Hydrogen production for energy: An overview, *International Journal of Hydrogen Energy*, 45(7), 3847 – 3869.

[6] B. Ahmed, M. B. Tahir, S. Nazir, M. Alzaid, A. Ali, M. Sagir & H. Alrobei, 2023. An Ab-initio simulation of boron-based hydride perovskites XBH_3 (X = Cs and Rb) for advance hydrogen storage system, *Computational and Theoretical Chemistry*, 1225, 114173.

[7] A. Siddique, A. Khalil, B. S. Almutairi, M. B. Tahir, M. Sagir, Z. Ullah, A. Hannan, H. E. Ali, H. Alrobei & M. Alzaid, 2023. Structures and hydrogen storage properties of $AeVH_3$ (Ae = Be, Mg, Ca, Sr) perovskite hydrides by DFT calculations, *International Journal of Hydrogen Energy*, 48(63), 24401 – 24411.

[8] M. Usman, J. ur Rehman, M. B. Tahir & A. Hussain, 2022. Structural, electronics, magnetic, optical, mechanical and hydrogen storage properties of Ga-based hydride-perovskites $XGaH_3$ (X = K, Li), *International Journal of*

Energy Research, 46(11), 15617 – 15626.

[9] A. Rafique, M. Usman, J. U. Rehman, A. Nazeer, H. Ullah & A. Hussain, 2023. Investigation of structural, electronic, mechanical, optical and hydrogen storage properties of cobalt-based hydride-perovskites $XCoH_3$ (X = In, Mn, Sr, Sn, Cd) for hydrogen storage application, *Journal of Physics and Chemistry of Solids*, 181, 111559.

[10] N. Xu, Y. Chen, S. Chen, S. Li & W. Zhang, 2024. First-principles investigation for the hydrogen storage properties of $XTiH_3$ (X=K, Rb, Cs) perovskite type hydrides, *International Journal of Hydrogen Energy*, *50,* 114 – 122.

[11] A. M. Ali, B. Azeem, S. Akbar, A. Saddiqa, M. Ahmad, S. Rehman, M. H. Rahman & A. B. Mahpudz, 2025. A DFT investigation of Li-based hydride perovskites $LiXH_3$ (X = S, Se) for hydrogen storage applications, *International Journal of Hydrogen Energy*, 154, 150299.

[12] M. R. Talukder & M. R. Islam, 2025. Effect of transition metal on the physical and hydrogen storage properties of the dynamically stable novel $ARhH_3$ (A = Mg, Ca, and Sr) hydrides for solid-state hydrogen storage application: A DFT and AIMD study, *Fuel Processing Technology*, 277, 108312.

[13] A. Hammad, T. A. Geleta, M. Ali & N. Bouri, 2025. Exploring Zr-based perovskite hydrides $XZrH_3$ (X: Na/Cs) for hydrogen storage applications: Insights from first-principles DFT calculations, *International Journal of Hydrogen Energy*, 126, 22 – 35.

[14] B. Ahmed, M. Bilal Tahir, M. Sagir, A. Parveen, Z. Abbas & K. M. Al-Aiban, 2025. Unveiling the potential of $XInH_3$ (X = Rb and Cs): A DFT study for solid state hydrogen storage applications, *Chemical Physics*, 588, 112441.

[15] A. Koufi, Y. Ziat & H. Belkhanchi, 2025. First-principles DFT and BoltzTraP investigation of multifunctional properties of $XNiH_3$ (X = Li, Na, K) perovskite hydrides: Thermoelectric and hydrogen storage potential, *Next Energy*, 9, 100402.

[16] A. Afaq, M. Alam, H. B. Munir, A. Bakar & H. E. Ali, 2025. Structural, electronic, phonon, thermodynamic and hydrogen storage properties of $BeXH_3$(X = Si,Ge) Hydride Perovskites: A DFT approach, *International Journal of Hydrogen Energy*, 127, 127 – 136.

[17] N. Marzari, D. Vanderbilt & M. C. Payne, 1997. Ensemble Density-Functional Theory for *Ab Initio* Molecular Dynamics of Metals and Finite-Temperature Insulators, *Physical Review Letters*, 79(7), 1337.

[18] D. Vanderbilt, 1990. Soft self-consistent pseudopotentials in a generalized eigenvalue formalism, *Physical Review B*, 41(11), 7892.

[19] H. Xu & D. Guan, 2022. Exceptional Anisotropic Noncovalent Interactions in Ultrathin Nanorods: The Terminal σ-Hole, *ACS Applied Materials and Interfaces*, 14(45), 51190 – 51199.

[20] J. U. Rehman, M. Usman, S. Amjid, M. Sagir, M. B. Tahir, A. Hussain, I. Alam, R. Nazir, H. Alrobei, S. Ullah & M. A. Assiri, 2022. First-principles calculations to investigate structural, electronics, optical and elastic properties of Sn-based inorganic Halide-perovskites $CsSnX_3$ (X = I, Br, Cl) for solar cell applications, *Computational and Theoretical Chemistry*, 1209, 113624.

[21] S. Berri, 2018. Ab initio study of fundamental properties of $XAlO_3$ (X = Cs, Rb and K) compounds, *Journal of Science: Advanced Materials and Devices*, 3(2), 254 – 261.

[22] G. Surucu, A. Gencer, A. Candan, H. H. Gullu & M. Isik, 2020. $CaXH_3$ (X = Mn, Fe, Co) perovskite-type hydrides for hydrogen storage applications, *International Journal of Energy Research*, 44(3), 2345 – 2354.

[23] N. A. Md Nasir, 2022. *First principles study on properties and voltages of cathode material nickel doped prussian blue for sodium ion battery* [Doctoral dissertation, Universiti Teknologi MARA (UiTM)].

[24] M. K. Masood, W. Khan, S. Bibi, A. Kanwal, S. Bibi, G. Noor, A. A. Alothman, J. Rehman & S. A. Shafiee, 2024. Physical properties of the $XScH_3$ (X: Ca, and Mg) perovskite hydrides and their hydrogen storage applications, *Journal of Physics and Chemistry of Solids*, 192, 112098.

[25] R. Song, Y. Chen, S. Chen, N. Xu & W. Zhang, 2024. First-principles to explore the hydrogen storage properties of $XPtH_3$ (X=Li, Na, K, Rb) perovskite type hydrides, *International Journal of Hydrogen Energy*, 57, 949 – 957.

[26] M. K. Masood, W. Khan, K. Chaoui, Z. Ashraf, S. Bibi, A. Kanwal, A. A. Alothman & J. Rehman, 2024. Theoretical investigation of $XSnH_3$ (X: Rb, Cs, and Fr) perovskite hydrides for hydrogen storage application, *International Journal of Hydrogen Energy*, 63, 1248 – 1257.

[27] S. Hayat, R. M. Arif Khalil, M. I. Hussain, A. M. Rana & F. Hussain, 2021. Ab-initio study of the structural, optoelectronic, magnetic, hydrogen storage properties and mechanical behavior of novel combinations of hydride perovskites $LiXH_3$ (X = Cr, Fe, Co, & Zn) for hydrogen storage applications, *Journal of Computational Electronics*, 20(6), 2284 – 2299.

[28] S. M. Deen, M. Usman, J. U. Rehman, S. A. Mansoor & M. Ali, 2024. A DFT study for physical properties and hydrogen storage capability of indium-based hydride perovskites $XInH_3$ (X = Li, K) for hydrogen storage application, *Solid State Communications*, 384, 115488.

[29] N. Ghaffar, M. Usman, J. U. Rehman, A. Hussain, S. M. Ali & M. Ali, 2024. A DFT study to investigate physical properties and hydrogen storage capability of Mn-based hydride perovskites $XMnH_3$ (X = Ba, Ca) for hydrogen storage application, *Inorganic Chemistry Communications*, 161, 112167.

[30] A. Mera & M. A. Rehman, 2024. First-principles investigation for the hydrogen storage properties of $AeSiH_3$ (Ae = Li, K, Na, Mg) perovskite-type hydrides, *International Journal of Hydrogen Energy*, 50, 1435 – 1447.

[31] N. Xu, Y. Chen, S. Chen, W. Zhang, S. Li, R. Song & J. Zhang, 2023. First-principles investigations for the hydrogen storage properties of XVH_3 (X=Na, K, Rb, Cs) perovskite type hydrides, *Journal of Materials Research and Technology*, 26, 4825 – 4834.

[32] R. M. A. Khalil, S. Hayat, M. I. Hussain, A. M. Rana & F. Hussain, 2021. DFT based first principles study of novel combinations of perovskite-type hydrides $XGaH_3$ (X = Rb, Cs, Fr) for hydrogen storage applications, *AIP Advances*, 11(2).

[33] J. Yang, A. Sudik, C. Wolverton & D. J. Siegel, 2010. High capacity hydrogen storage materials: attributes for automotive applications and techniques for materials discovery, *Chemical Society Reviews*, 39(2), 656 – 675.

[34] A. Farid, J. Fatima, E. Aldosari, I. Shahid & A. Ullah, 2025. Exploring the physical properties of the perovskite-type hydrides $NaXH_3$ (X = Ni, Cu, Zn) for hydrogen storage applications: A DFT study, *Structural Chemistry*, 36(5), 1765 – 1777.